This is a pre-print of the paper published by Elsevier in Tribology International, Vol. 82 part B (2015) p. 375-386
kris@kubiak.co.uk https://doi.org/10.1016/j.triboint.2014.04.035

Identification of lubrication regime on textured surfaces by multi-scale decomposition

C. Hubert[a,b,*], K. J. Kubiak[c], M. Bigerelle[a,b], A. Dubois[a,b], L. Dubar[a,b]

[a]*Univ Lille Nord de France, F-59000 Lille, France* [b]*UVHC, TEMPO EA 4542, F-59313 Valenciennes, France Telephone: +33 3 27 51 14 54, Fax: +33 3 27 51 13 17*
[c]*University of Liverpool, School of Engineering, Liverpool L69 3GH, United Kingdom*

Abstract

This paper focuses on the analysis of surfaces resulting from thickness reduction of aluminium strips, provided with lubricant reservoirs, and deformed with different lubricant viscosities and drawing velocities, by a specific experimental drawing process. During reduction, the lubricant is pressurized and may escape from its initial cavities and supply the neighbouring ones. The nature of the lubrication regime is thus locally changed and may vary from boundary to hydrodynamic. The deformed surfaces are measured by means of a Vertical Scanning Interferometer then analysed in terms of arithmetic roughness and developed roughness profile length. Since these two parameters are found not accurate enough to identify regions where different lubrication phenomena occurred, a method based on roughness peaks and valleys curvature radii estimation, recently developed by some of the present authors, is applied.

The acquired surfaces are assumed as fractal surfaces and a multiscale decomposition of the peaks and valleys curvature radii of roughness profile is performed, for each experimental test. Then the analysis of the deformed surfaces is achieved and the effects of the different testing conditions on the curvature radii are highlighted. During this study, this method has been of great help to qualitatively define the different contacts nature, *i.e.* severe or not, and to link the different regions to a lubrication regime.

Keywords: Roughness, Friction, Curvature radius, Fractal

1. Introduction

Metal forming operations generally require mixed lubrication regime to reduce the friction at the tool/workpiece interface and to improve the visual aspect and roughness of the final surfaces [1]. The peculiarity of this lubrication regime lies in the fact that only the

micro-cavities, inherent from surfaces roughness [2], are filled with lubricant during the contact, and thus the peaks of both surfaces are in dry contact. In plane strain processing, when plastic deformation occurs, the cavities filled with lubricant are pressurized and release the lubricant towards the drawing direction or in the opposite direction, according to the involved phenomena: Micro Plasto HydroStatic Lubrication (MPHSL, governed by the pressure gradient between the cavity and the contact pressure) or Micro Plasto HydroDynamic Lubrication (MPHDL, mainly governed by the relative speed between the tool and the worked surface), respectively. The result of this lubricant escape is a local change of lubrication regime that may become hydrodynamic rather than the initially expected, mixed lubrication regime.

The concept of Micro Plasto Hydrodynamic Lubrication (MPDHL) was first proposed by Mizuno and Okamoto [3] and later by Kudo et al. [2]. Azushima et al. [4] and Bech et al. [5] proved it in plane strain drawing of aluminium strips on which pyramidal indentations were manufactured and filled with lubricant. The lubricant dynamic behaviour was observed through a transparent glass die and recorded by means of a video camera. The aim of the latter study was to determine the drawing parameters, such as the lubricant viscosity, drawing speed, back tension or friction coefficient, that lead to MPHSL and/or MPHDL. This study also showed strong changes in the worked surface roughness where MPHSL and MPHDL occur, but has not been investigated further. More recently, Dubar et al. [6] carried out similar kind of experiments, with the same testing device as [5], but with triangular sectioned grooves as lubricant reservoirs, machined by means of Electro Discharge Machining (EDM). The aim of this technique was to avoid metal banks due to the indentation process, to avoid any lubricant escape perturbation due to these banks and to confer true plane strain properties to the analysis, including the lubricant escape. The drawing parameters investigated in this study were the drawing speed, the lubricant viscosity and the pockets angle to the edge, with goal to model numerically the lubricant reservoirs depth reduction due to plastic deformation and subsequent fluid escape during drawing, by means of a Fluid Structure Interaction model. Other studies focusing on related phenomena in drawing process like friction, lubrication, roughness etc. have been carried out [7–11]. In the present study, the experimental results produced by Dubar et al. [6] are used to analyse the effects of lubricant escape on the final roughness of the worked surfaces.

As classical tribological parameters such as the arithmetic roughness (R_a) or the developed profile length (R_{L0}) do not allow clear identification of regions where different phenomena occur [12], the method based on roughness peaks curvature estimation, which plays an important role in contact pressure, recently developed by Bigerelle et al. [12] is applied. This method considers the specimens surfaces as fractal surfaces and thus allows to perform a multiscale decomposition of this radius of curvature. Even if the calculation of the radius of curvature requires smooth surfaces, it is not always the case when dealing with fractal surfaces, as shown by Mandelbrot and Wallis [13]. Moreover, as all metric parameters relative to fractal curve depend on the measurement scale, it becomes difficult to give a physical sense of the local radius of curvature for fractal surfaces. And if in tribology contact fractal surfaces are often used to avoid sensitivity of the measurement scale, this approach is used

This is a pre-print of the paper published by Elsevier in Tribology International, Vol. 82 part B (2015) p. 375-386
kris@kubiak.co.uk https://doi.org/10.1016/j.triboint.2014.04.035

here to identify the regions where different contact conditions occurred, especially a local change in lubrication regime due to either MPHSL or MPHDL.

The present paper is divided into three parts. Firstly, the experimental tests carried out are described: the testing device functioning is detailed as well as the specimens preparation and properties, and the testing conditions. Then the methodology for the acquisition of the worked specimens topographical information is explained. Secondly the methodology to perform the whole multiscale decomposition of the radius of curvature along a given topographical profile is described. Then, based on the prior multiscale decomposition, the analysis of the results is carried out to quantify the effects of the experimental process parameters (*i.e.* the lubricant viscosity, the drawing velocity and the pockets angle) on the radius of curvature measured on the final surfaces. Finally the link between this radius of curvature and the lubrication regime is presented, with comparisons to regions outside of the pockets row and to initial profiles. The results are then discussed and proposals for future works are given.

2. Experimental tests and surfaces topography acquisition

2.1. Testing device and design of experiments

The experimental testing device used in this study has been developed by Bech et al. [5] for thickness reduction of aluminium strips. The strips are drawn by means of a hydraulic jack between two dies: the upper one is made of hardened glass so the lubricant behaviour can be observed during thickness reduction, and the lower die is made of steel with an inclined plane with angle $\beta = 3^{\circ}$ to apply the thickness reduction. The hardened glass is used as delivered in shape of circular disc of dimensions ⌀50 × 11 mm, and the lower die is 80 mm long and 50 mm wide, with polished contacting surface to reduce friction. A high speed video camera is used to record the lubricant behaviour for subsequent analysis, *i.e.* identification of the occurrence of MPHSL and MPHDL, location of the onset and direction of escape or front wave speed. The testing device is illustrated in figure 1.

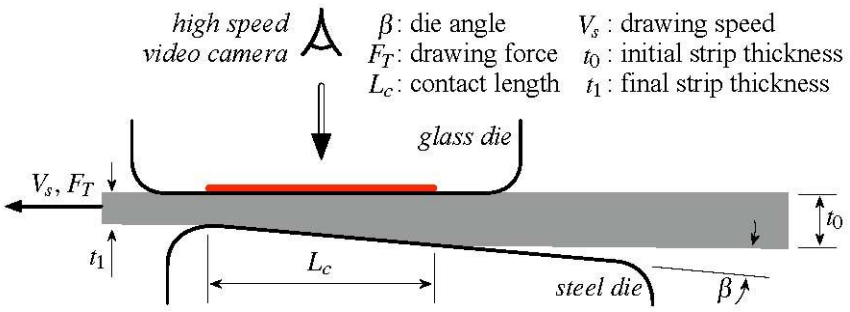

Figure 1: Experimental testing device with its intrinsic parameters [14].

The provided strips dimensions are $l_0 \times L_0 \times t_0 = 450 \times 20 \times 2$ mm and their material is a semi-hardened aluminium AISI 1050 H24. Macro lubricant pockets are manufactured by 3

This is a pre-print of the paper published by Elsevier in Tribology International, Vol. 82 part B (2015) p. 375-386
kris@kubiak.co.uk https://doi.org/10.1016/j.triboint.2014.04.035

means of Electro Discharge Machining to reduce the local residual stresses and to avoid the formation of banks that would change the tribological contact properties and fluid escape, as observed in a prior study [15]. The shape of the lubricant pockets is a groove normal to the drawing direction with triangular cross section. They are 10 mm long and 1 mm wide, with an angle to the edge $\alpha = 5^{\circ}$ for the first set of specimens, and $\alpha = 10^{\circ}$ for the second one. The spacing between each cavity centre is 2 mm, so that the plateaus are 1 mm wide. The strips are obtained from cold rolling and their raw roughness is preserved all along the specimens preparation process. An illustration of the manufactured strips and an illustrative picture are given in figure 2.

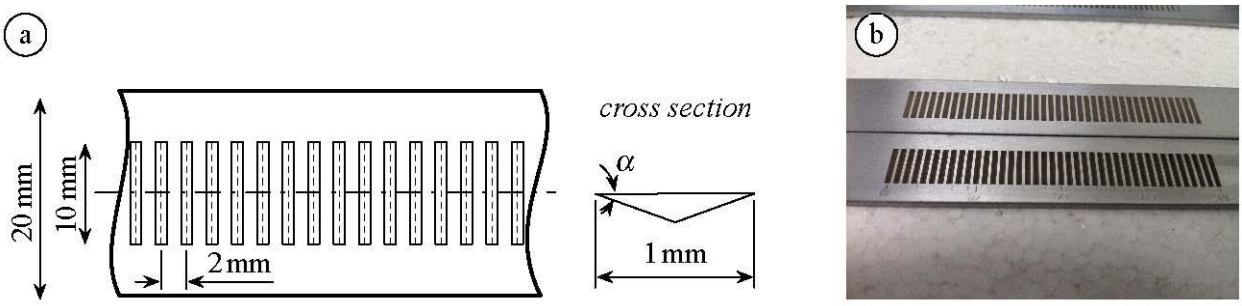

Figure 2: Groove shaped pockets pattern (a) and picture (b) of two EDM processed strips.

In the experiments carried out for this study several testing conditions are applied to analyse the sensitivity of the lubrication phenomena described above, *i.e.* MPHSL and MPHDL: the pockets angle to the edge applied during the EDM of the specimens ($\alpha = 5^{\circ}$ and $\alpha = 10^{\circ}$), the lubricant, which is a pure mineral oil with two viscosities (η = 60 cSt and η = 660 cSt at 40 °C) and the drawing velocity (V_s =5 mms^{-1} and V_s = 50 mms^{-1}). All these parameters are crossed together so that eight experimental conditions are tested, each testing condition being tripled resulting in twenty four tests. The design of experiments is summed up in table 1 along with the name assigned to each testing condition (*e.g.* 5DTC1 means 5 Degrees, Testing Condition 1).
During testing global parameters are recorded such as the drawing speed, drawing force, and the lubricant dynamic behaviour by means of a high speed video camera set to a frame rate of f_r = 125 fps when drawing at V_s =5 mms^{-1}, and f_r = 1500 fps at V_s = 50 mms^{-1}.

2.2. Deformed surfaces topography acquisition

The surfaces topography were acquired using a Zygo NewView 7300 [16] profilometer which is a Vertical Scanning Interferometer (VSI). The measurement principle is that unfiltered white light beam is split in two: half of the beam is directed through a microscope lens and reflected from the surface, and the other half is reflected from the reference mirror. When reflected beams combine together they produce interference fringes, where the best-contrast fringe occurs at best focus. In VSI mode the objective moves vertically to scan the

This is a pre-print of the paper published by Elsevier in Tribology International, Vol. 82 part B (2015) p. 375-386
kris@kubiak.co.uk https://doi.org/10.1016/j.triboint.2014.04.035

Table 1: Testing conditions and corresponding condition name.

Pocket angle	Drawing velocity	Lub. viscosity (40°C)	Condition Name
α = 5°	V_s = 5 mm s^{-1}	η = 60 cSt	5TDC1
		η = 660 cSt	5TDC2
	V_s = 50 mm s^{-1}	η = 60 cSt	5TDC3
		η = 660 cSt	5TDC4
α = 10°	V_s = 5 mm s^{-1}	η = 60 cSt	10TDC1
		η = 660 cSt	10TDC2
	V_s = 50 mm s^{-1}	η = 60 cSt	10TDC3
		η = 660 cSt	10TDC4

surface at various heights. A 3D surface is then reconstructed by analysis of fringes at every pixel. VSI mode uses an algorithm to process fringe modulation data from the intensity signal to calculate the surface heights. The obtained resolution will therefore depend on the precision of the z-axis positioning. In the case of the Zygo NewView 7300 instrument a piezoelectric stage with range of 160µm is used to refine the height resolution going down to 0.1 nm. The spatial resolution depends on the camera size and the used lens; in our case the surfaces were acquired then stitched together to cover an area of 8 × 2 mm^2 with spatial resolution (x, y) of 1.1µm [14]. The location of the measurements is chosen so that both deformation and lubrication regimes are stabilized. It starts at the 15th pocket, in the middle of the strip as illustrated in figure 3.

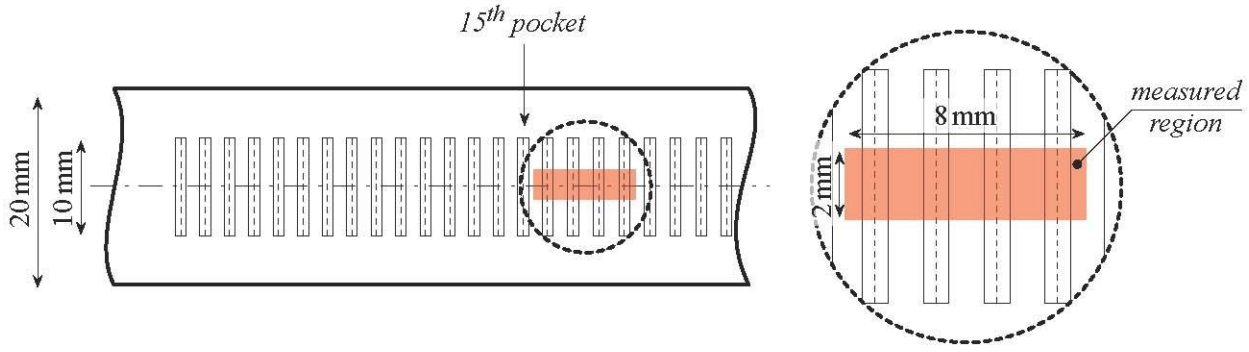

Figure 3: Illustration of measurements location and extent.

An example of surface measured before drawing is given in figure 4a. It clearly shows the characteristic topography of cold rolling with strias in the working direction (x-axis) on the plateaus (regions of the surface at zero height) and rough, dull surface state in the lubricant pockets due to the EDM.

On the surfaces measured after drawing (figure 4b) the strias due to cold rolling have

This is a pre-print of the paper published by Elsevier in Tribology International, Vol. 82 part B (2015) p. 375-386
kris@kubiak.co.uk https://doi.org/10.1016/j.triboint.2014.04.035

been flattened and the resulting plateaus surface is smoother than the original surface. It can also be observed that the shape of the lubricant pockets has changed after processing, and two new regions can be identified, labelled 2 and 4 (figure 4b). Initially, those surfaces belonged to the lubricant pockets and, due to elastoplastic deformation, they now form part of a plateau. It is however assumed that because of the large amount of lubricant in this region, the contact was only partial and thus the topography of regions 2 and 4 is similar to that of the pockets, labelled 1.

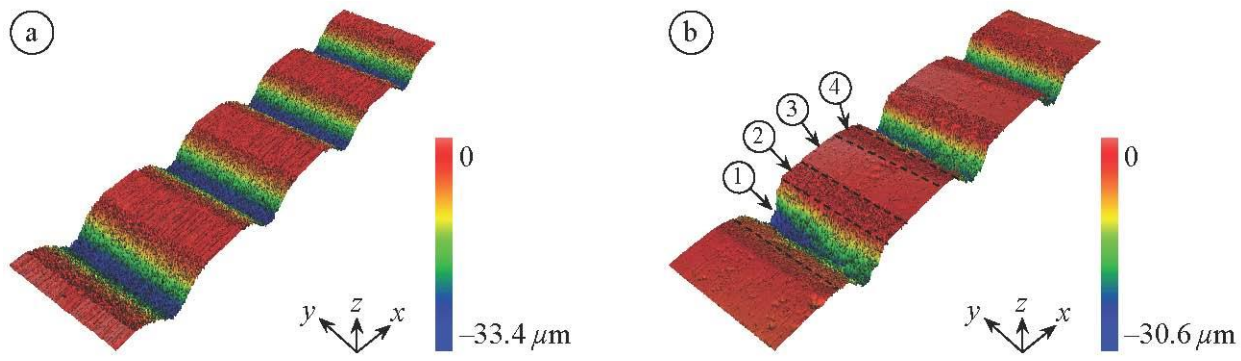

Figure 4: Illustration of strips surfaces before (a) and after (b) drawing.

In this kind of deformation process, the surface roughness will change leaving a specific signature of tribological process that can be revealed with an analysis of the surface roughness. However, direct analysis of 3D surface morphology is computationally more expensive and less robust than 2D analysis in the case of pure anisotropic surfaces. Therefore, to analyse surface roughness, a specific technique of transition from 3D surface to 2D surface profiles analysis has been developed. Given a 3D surface, it consists in generation of series of 2D profiles in the y-direction of this surface. Once the profiles are extracted, different parameters can be calculated from individual profiles such as the classical arithmetic roughness or the developed length of the roughness profile, as described in [12] and illustrated in figure 5. Though, as described in [12], using a simple amplitude parameter such as the arithmetic roughness (R_a) can not clearly distinguish all contacting regions. The developed length of roughness profile (R_{L0}) is able to distinguish them with slight variations, but is not clear enough to perform a reliable analysis.

This is a pre-print of the paper published by Elsevier in Tribology International, Vol. 82 part B (2015) p. 375-386
kris@kubiak.co.uk https://doi.org/10.1016/j.triboint.2014.04.035

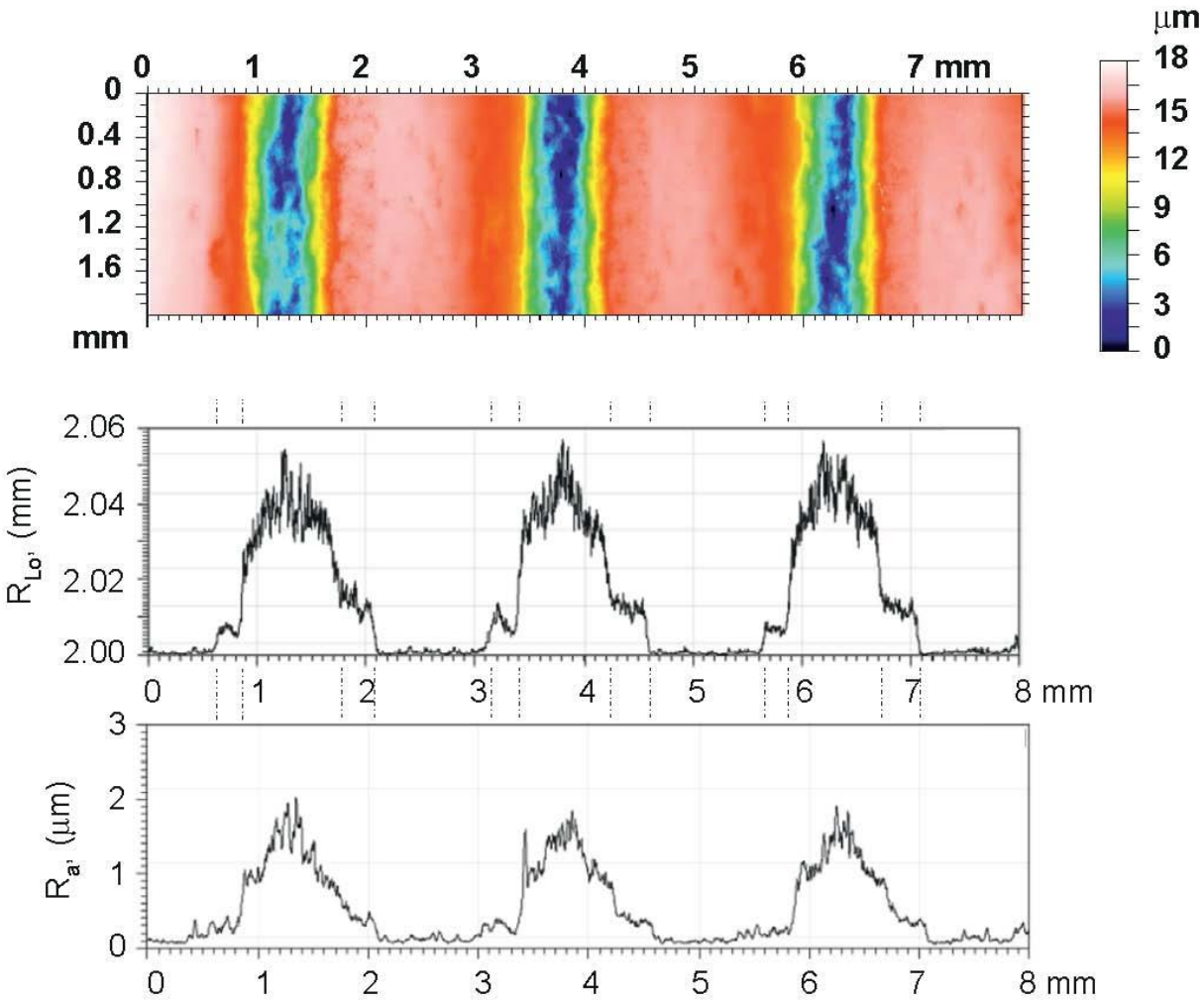

Figure 5: Roughness parameters R_a and R_{L0} calculated on individual profiles, extracted in y-direction from the 3D surface [12].

Thus, an algorithm has been developed to estimate the radius of curvature of a fractal curve and to establish the dependency of this radius on the scale at which the surface is observed and its relationship with the fractal dimension of this surface. This work is fully detailed in [12] and the main lines are given in section 3.1.

This is a pre-print of the paper published by Elsevier in Tribology International, Vol. 82 part B (2015) p. 375-386
kris@kubiak.co.uk https://doi.org/10.1016/j.triboint.2014.04.035

3. Multiscale decomposition of profile curvature radius

3.1. Methodology

According to Nowicki [17], it is possible to study the roughness of a given surface by introducing a parameter called *radius of asperity*, which is determined by the relation

$$r_c = l_x^2/8l_y \qquad (1)$$

where r_c is the radius of a circle with centre O, passing by a crest A and by two points B and C of the profile. l_x corresponds to the distance between points B and C, l_y is the distance between line (B, C) and line (B, C) and the circle centre O. l_y is considered sufficiently small so that segment [A, O] is supposed to be perpendicular to segment [B, C], in its middle I. These parameters are illustrated in figure 6 on a regular profile.

point A, andthedistance $r_c - l_y$ correspondstoth edistancebetwe en

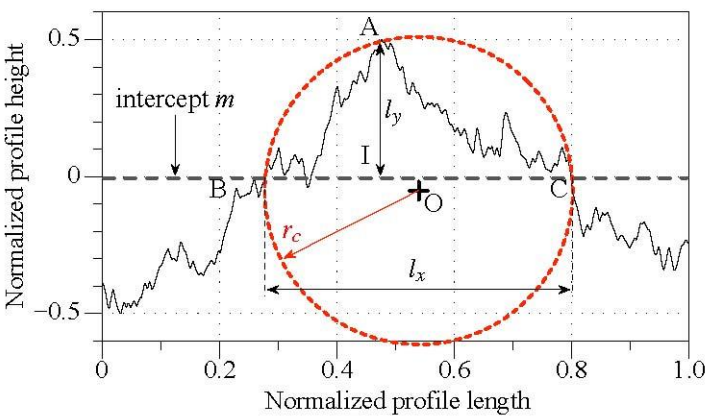

Figure 6: Definition of parameters used to calculate the local radius of curvature (after [12]).

Equation 1 is obtained by assuming that l_y is sufficiently small so that condition $l_y << l_x$ is satisfied.

For fractal curves, r_c depends on the scale at which the observation is made, and as we postulate that the curvature radius can be defined at a given scale, the parameter l_x is assumed to be the measurement scale, calculated as follows:

This is a pre-print of the paper published by Elsevier in Tribology International, Vol. 82 part B (2015) p. 375-386
kris@kubiak.co.uk https://doi.org/10.1016/j.triboint.2014.04.035

1. A horizontal straight line is chosen at a given level h that crosses the measured profile and a set of values of l_x is built with the intersections of the straight lines intercepting the profile.
2. For each value of l_x the local maximum peak (*i.e.* the maximum value of the profile) is obtained, giving the corresponding value of l_y.
3. The curvature radius of the peak r_c is calculated according to equation 1.
4. The sequence (1–3) is repeated m times for m other horizontal straight lines chosen randomly.

Experimentally, the fractal dimension Δ is obtained as a slope by fitting the discretised data of the function $\log r_c(l_x) = f(\log l_x)$ obtained by the algorithm described above. If the regression line fit well (usually with a coefficient of correlation R ranging in [0.95, 1]), the experimental data then allow writing the scale law

$$r_c(l_x) = \lambda l_x^{\Delta}. \quad (4)$$

The multiscale decomposition will be performed by means of this scale law.

3.2. Application on an initial profile

The algorithm is introduced with a 2D profile while the acquired data are surfaces, and thus 3D. Meanwhile the experimental tribotest used for this study performs plane strain deformations, which means that the mechanical behaviour of the specimens is (theoretically) identical whatever the observation position in the width direction. As done for parameters R_a and R_{L0} (figure 4), the algorithm will be applied on all profiles in the width direction and theobtainedvalueofthecurvatureradiusofpeakswillbereportedona $\log r_c(l_x) = f(x_{profile})$ graph for several values of the measurement scale $\log l_x$, ranging from 0.35 to 3.0.

As discussed earlier, the radii of curvature of the profile peaks are an important indicator of contact severity and thus contact pressure. In the same way as developed, another important indicator may be the radius of curvature of valleys: it is clear that for soft to medium contact the curvature radius of peaks will change, but the curvature radius of valleys won't change significantly. On the contrary for severe contact conditions, the peaks will flatten leading to increased curvature radius, as well as the valleys. To compute the radius of the profile valleys, the same algorithm as for the peaks is applied after initial transformation of the surface z(x, y) into −z(x, y).

Finally, still based on the radii of curvature of peaks and valleys, a third indicator will be useful for the interpretation of the results: the dimensionless ratio R between the radius of curvature of peaks and the radius of curvature of valleys, expressed as

$$R = \frac{r_{cP}}{r_{cV}}, \quad (5)$$

with r_{cP} and r_{cV} the radii of curvature of peaks and valleys, respectively. In logarithmic scale, as it will be used in the remainder of this paper, this indicator becomes

$$R^{\diamond} = \log R = \log r_{cP} - \log r_{cV}. \quad (6)$$

Three main values can be considered for this indicator:

This is a pre-print of the paper published by Elsevier in Tribology International, Vol. 82 part B (2015) p. 375-386
kris@kubiak.co.uk https://doi.org/10.1016/j.triboint.2014.04.035

1. $R^{\diamond} > 0$: the radius of peaks is greater than that of valleys, meaning that the peaks have been eroded but not the valleys. The other way may also be considered, *i.e.* r_{cV} becomes smaller without change for r_{cP} , but it seems to be inconsistent since any process starts by eroding the peaks then the valleys, except if the valleys are filled with third body particles, created by the tool/workpiece friction and wear.
2. $R^{\diamond} = 0$: means that both radii of curvature (peaks and valleys) are equal.
3. $R^{\diamond} < 0$: the peaks curvature radius has been reduced or that of the valleys has been increased.

These three indicators, namely the peaks curvature radius, the valleys curvature radius and the ratio between these last two curvature radii have been computed for the initial strip illustrated in figure 4a, and reported in figure 7, along with a top view of the surface topography and a 2D profile of this surface, taken in its middle.

This is a pre-print of the paper published by Elsevier in Tribology International, Vol. 82 part B (2015) p. 375-386
kris@kubiak.co.uk https://doi.org/10.1016/j.triboint.2014.04.035

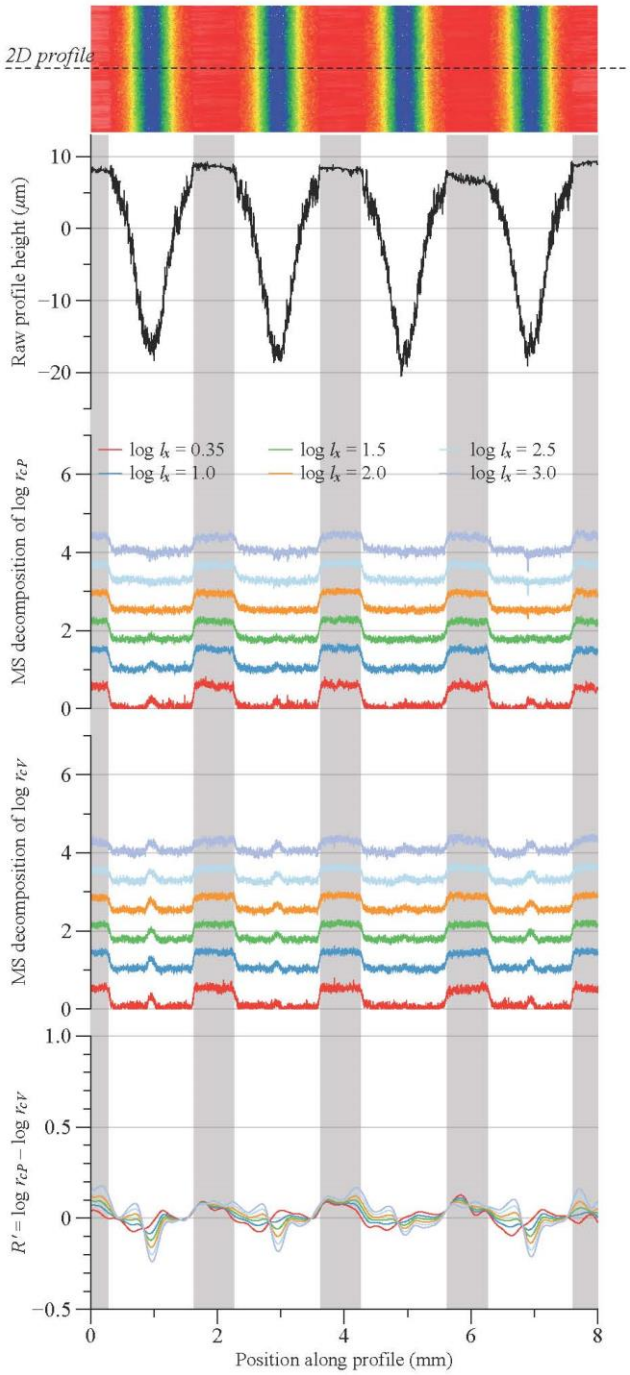

Figure 7: Multiscale decomposition of peaks and valleys curvature radii and parameter R' for an initial strip with pockets angle of 10° .

It can be seen on the graph of figure 7 that the curvature radii of peaks r_{cP} and valleys r_{cV} are very close, if not equal. The analysis and explanations of the different parameters is

given below:

- Logically, regions that have been cold rolled have high curvature radii since cold rolling apply large plastic deformation to the strips leading to important flattening of both peaks and valleys. Moreover, the work rolls being much harder than the aluminium strip, they transfer their roughness, which is typical of rolls grinding, to the worked strips.
- The regions affected by the Electro Discharge Machining also have similar value of curvature radii of peaks and valleys, but this value is smaller than that encountered for the strips plateaus. The EDM actually removes aluminium particles almost uniformly instead of flattening the strip surface.
- For both regions, the ratio $R^{\blacklozenge}$ of peaks and valleys curvature radii (equation 6) is thus close to zero, ranging from −0.2 to +0.2 for all measurement scales.

These values of the peaks and valleys curvature radii and ratio for this initial profile will be kept as reference values for the next analysis of the measurements performed after drawing.

3.3. Determination of the most relevant analysis scale The major interest and key for the following study is to find the scale *i.e.* the l_x value at which the ratio $R^{\blacklozenge}$ of peaks and valleys curvature radii must be analysed. To determine this scale, appropriate statistical analyses are performed. For all profiles, all values of individual peaks and valleys curvature radii are taken into account, giving 452, 861, 509 peaks and 452, 861, 510 valleys, so about 9×10^8 asperities. From these analyses, it is decided to test if the difference between peaks and valleys is more significant for all measurement scale values l_x and this for all maps and all *x*-positions. Then analyses of variance are proceeded to find where is the more relevant measurement scale l_x from which difference between peaks and valleys curvature are more significant and thus all cases (horizontal *x*-position and each sample). Only the most significant values are retained. The mean value of F (Fisher variate of the analysis of variance) variation versus the measurement scale l_x (in logarithmic values) are plotted on the graph of figure 8. Higher F correspond to higher difference between peak and valley curvatures. As it can be observed in figure 8, two maximum values are reached: the first one around $\log l_x = 0.35$ ($l_x = 2.24\mu m$) and the second one around $\log l_x = 2.5$ ($l_x = 315.23\mu m$). These two measurement scale values are linked to the size of the asperities; the others represent

the macrotopography linked to the structuration of the specimens. As a consequence, to analyse effect of the topography, we will retain the measurement scale $\log l_x = 0.35$.

4. Analysis of the deformed surfaces and identification of lubrication regimes

This section concerns the analysis of the specimens after drawing, for all configurations detailed in table 1. It is divided into 3 sub-sections: the first one is dedicated to the analysis

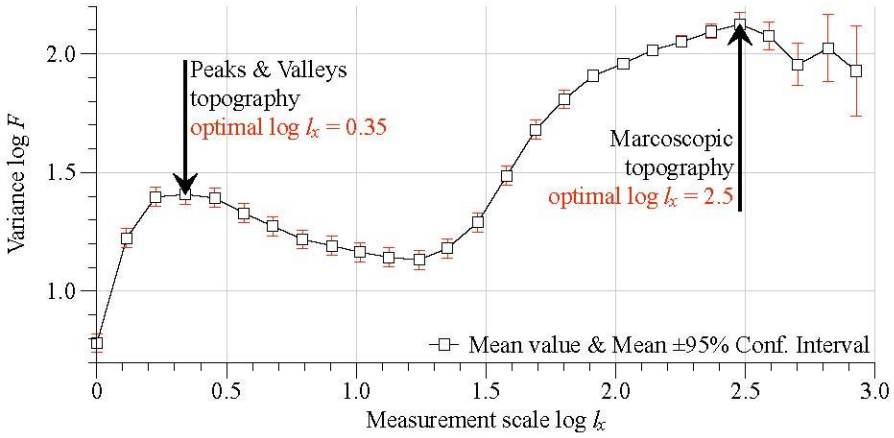

Figure 8: Determination of the most relevant scale to observe the multiscale decomposition.

of the effect of the lubricant viscosity, the second one will concern the drawing velocity and the third sub-section will finally be aimed at the identification of the different lubrication regimes that are encountered in this specific kind of tribological contact, by comparisons with measurements performed out of the pockets rows. The first two sub-sections will also deal with the effect of the pockets angle to the edge, which effects on the curvature radii are linked with that of the lubricant viscosity and the drawing velocity.

4.1. Effect of the lubricant viscosity

Generally, in mixed lubrication regime, increasing the lubricant viscosity allows to reduce the friction between the contacting surfaces and may favour a hydrodynamic lubrication regime. The expected effect of the high viscosity lubricant (η = 660 cSt) is thus smaller curvature radii for both peaks and valleys belonging to the strips plateaus (closer to the initial profiles) than for a low viscosity lubricant (η = 60 cSt). A comparison for testing conditions 5DTC1 and 5DTC2 is given in figure 9a and 9b, which correspond to low velocity tests with small and high lubricant viscosity, respectively. On this figure, it can be seen that, even if not constant, the value of log r_{cP} is higher for the low viscosity lubricant (5DTC1, figure9a)andrangesin [1.3, 1.8] ($r_{cP} \in$ [19.95, 63.1]µm), thanforthehighviscositylubricant (5DTC2, figure 9b), for which log $r_{cP} \approx 1.1$ ($r_{cP} \approx$ 12.59µm). The same observation can be made for the value of log r_{cV}, which ranges in [0.8, 1.3] ($r_{cV} \in$ [6.31, 19.95]µm) for η = 60 cSt and in [0.6, 1.1] ($r_{cV} \in$ [3.98, 12.59]µm) for η = 660 cSt.

This is a pre-print of the paper published by Elsevier in Tribology International, Vol. 82 part B (2015) p. 375-386
kris@kubiak.co.uk https://doi.org/10.1016/j.triboint.2014.04.035

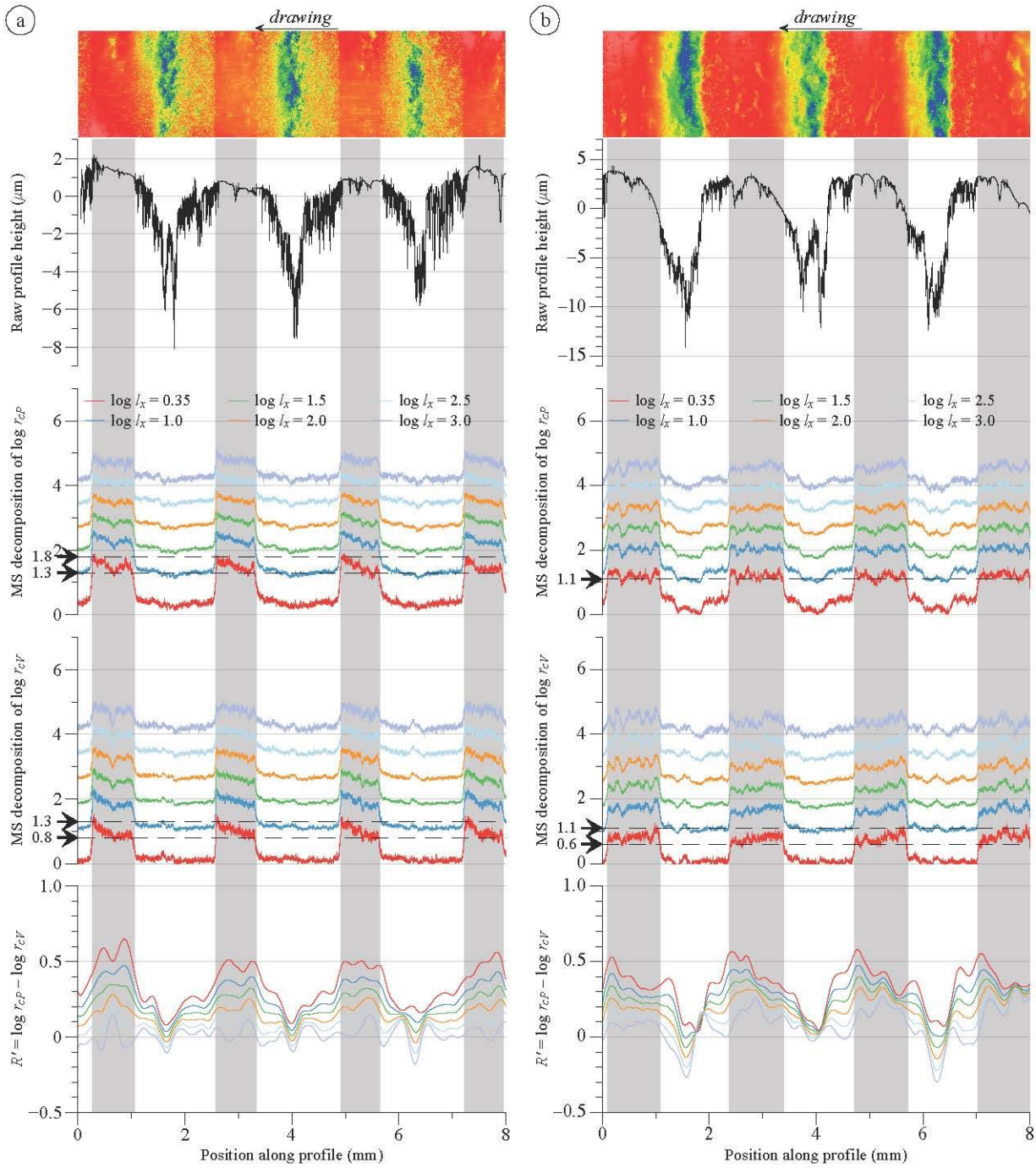

Figure 9: Multiscale decomposition of peaks and valleys curvature radii for conditions 5DTC1 (a) and 5DTC2 (b).

Still focusing on the strips plateaus, the same observations can be made for testing 14

This is a pre-print of the paper published by Elsevier in Tribology International, Vol. 82 part B (2015) p. 375-386
kris@kubiak.co.uk https://doi.org/10.1016/j.triboint.2014.04.035

conditions 5DTC3 and 5DTC4, that involve a high drawing velocity and low and high lubricant viscosities, respectively. For these configurations the radius of curvature of peaks is log $r_{cP} \approx 1.3$ ($r_{cP} \approx 19.95\mu m$) for the low viscosity lubricant while log $r_{cP} \approx 0.8$ ($r_{cP} \approx 6.31\mu m$) when using a high viscosity lubricant. For the valleys, log r_{cV} ranges in the interval [0.8; 1] ($r_{cV} \in [6.31, 10.00]\mu m$)fortestswithlowviscositywhile log $r_{cV} \approx 0.6$ ($r_{cV} \approx 3.98\mu m$) for tests with high viscosity lubricant.

Increasing the lubricant viscosity logically protects the contacting surfaces where the peaks contact pressure should be found smaller than for a low viscosity lubricant.

All tests performed with pockets angle $\alpha = 10^{\circ}$ (*i.e.* tests conditions names 10DTCx, x being the test combination) show the same trend: compared to the initial strips state (figure 7), the curvature radius of both peaks and valleys have much increased when using a low viscosity lubricant than when using a high viscosity lubricant. Meanwhile for $\alpha = 10^{\circ}$, theobservedcurvatureradiiareslightlyhigherthanforstripswithpocketsangle $\alpha = 5^{\circ}$, and especially for the peaks curvature radius. The multiscale decompositions for two identical running conditions but with two different angles are given in figure 10a and 10b, for $\alpha = 5^{\circ}$ and $\alpha = 10^{\circ}$ respectively.

Figure 10: Multiscale decomposition of peaks and valleys curvature radii for conditions 5DTC2 (a) and 10DTC2 (b).

This is a pre-print of the paper published by Elsevier in Tribology International, Vol. 82 part B (2015) p. 375-386
kris@kubiak.co.uk https://doi.org/10.1016/j.triboint.2014.04.035

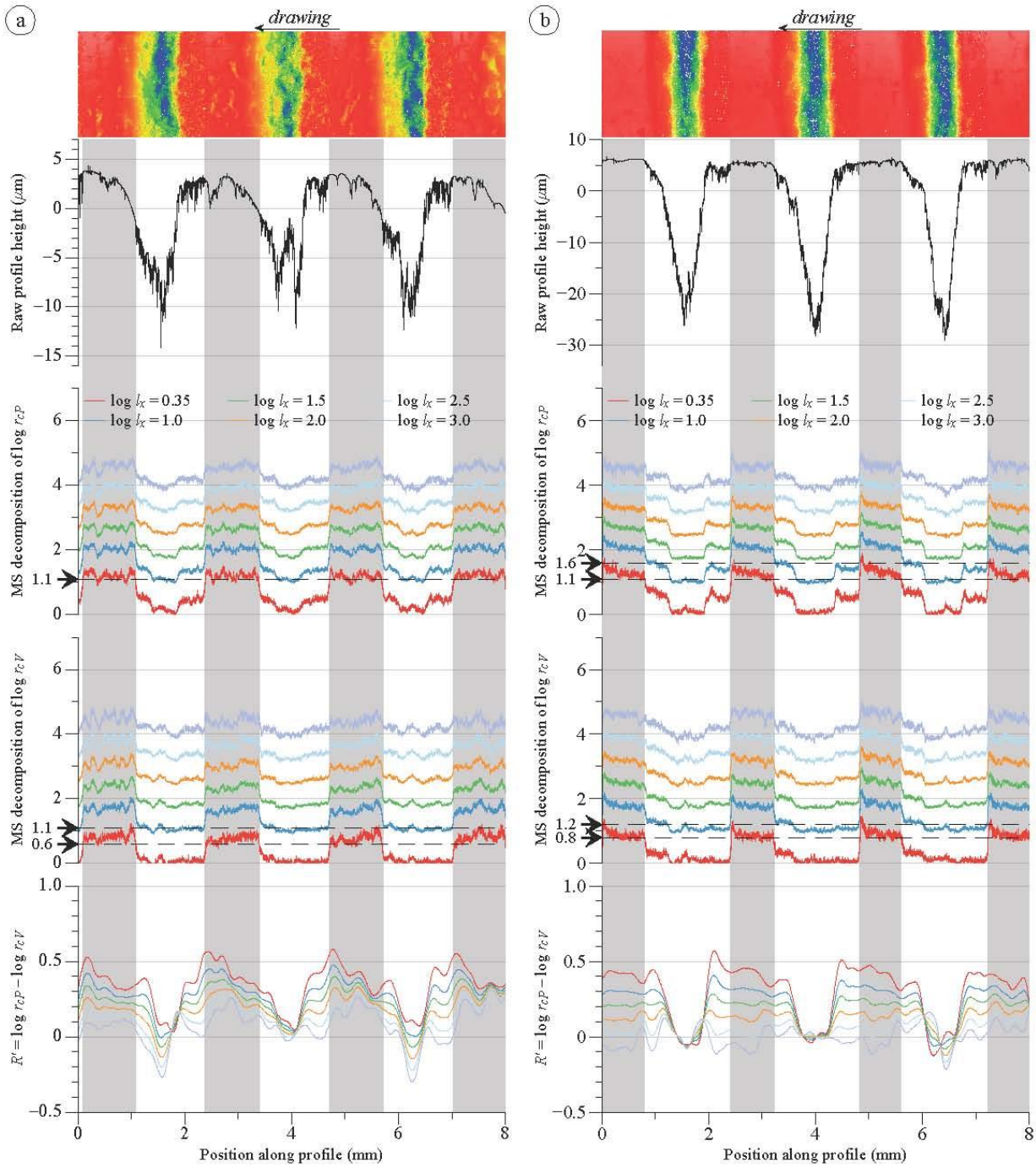

Figure 10: Multiscale decomposition of peaks and valleys curvature radii for conditions 5DTC2 (a) and 10DTC2 (b).

As postulated by Sørensen et al. [18], the angle to the edge of the lubricant reservoirs 16

plays an important role in the hydrodynamic part of contact lubrication. In their study, which is experimentally similar to that of Bech et al. [5] and to the present one, specimens provided with pyramidal indentations and several angles to the edge were drawn. The determinations of the onset of lubricant escape from the pockets by MPHDL showed that it occurred earlier for small pyramid angles than for high angles, which ranges from $\alpha = 3.6^{\circ}$ to $\alpha = 15^{\circ}$. Itthusleadstolesslubricantonthestripsplateausandmoreseveretool/workpiece contact.

The same phenomenon is observed in the present study and is highlighted by the curvature radii of peaks and valleys on the strips plateaus: MPHDL occurs later for pockets with $\alpha = 10^{\circ}$ than for pockets with $\alpha = 5^{\circ}$, with consequentially less lubricant on the strips plateaus, leading to more severe contact and thus, high curvature radii.
Moreover, the value of log r_{cP} is not only slightly higher for 10DTC2 than for 5DTC2, its profile is also different: it has a negative slope towards the +x-direction, that corresponds to the direction of MPHDL, while for the small pockets angle the profile of log r_{cP} is almost flat. As illustrated in figure 11, it means that the left border of the strips plateaus have undergone severe contact due to late lubrication. MPHSL, which is less sensitive to pockets angle do occurred and had lubricated the right part of the strips plateaus. In the case of configuration 5DTC2, MPHDL occurred earlier and both MPHSL and MPHDL melted to result in sufficient lubrication and almost uniform peaks radius of curvature on the strips plateaus.

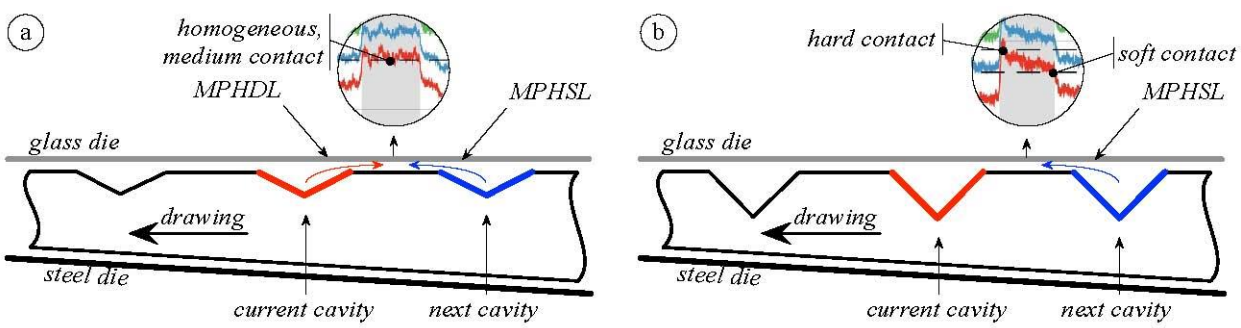

Figure 11: Illustration of the effect of the pockets angle to the edge on the evolution of the peaks curvatureе radius of the strips plateaus on configurations 5DTC2 (a) and 10DTC2 (b).

4.2. Effect of the drawing velocity

The drawing velocity also plays an important role in contact lubrication: as stated by Sørensen et al. [18] or Bech et al. [5], it increases the pressure in the lubricant pocket which overcomes the contact pressure (also called *sealing pressure*) and thus helps the lubricant to be dragged out of the cavity. In the case of the experiments carried out in this study, this effect can also be observed and, since a hydrodynamic lubrication regime tends to preserve the surfaces roughness, the observed final curvature radii are closer to the initial ones than for the tests performed at low velocity.

This is a pre-print of the paper published by Elsevier in Tribology International, Vol. 82 part B (2015) p. 375-386
kris@kubiak.co.uk https://doi.org/10.1016/j.triboint.2014.04.035

For strips with pockets angle α =5°, log r_{cP} ≈ 1.3 (r_{cP} ≈ 19.95µm, while 1.3 ≤ log r_{cP} ≤ 1.8, 19.95 ≤ r_{cP} ≤ 63.1µm at low velocity) for the low viscosity lubricant and is reduced to log r_{cP} ≈ 0.8, r_{cP} ≈ 6.31µm(log r_{cP} ≈ 1.1, r_{cP} ≈ 12.59µm at low velocity) with the high viscosity lubricant, which is consistent with the analysis given in the previous section. The same trend is observed for the curvature radius of valleys. log r_{cV} now ranges in [0.8, 1] ([6.31, 10.00]µm) instead of [0.8, 1.3] ([6.31, 19.95]µm) at low velocity and low viscosity, and it is reduced to log r_{cV} ≈ 0.6 (r_{cV} ≈ 3.98µm) with the high viscosity lubricant. This last value is very close to that of the initial profile, illustrated in figure 7, and clearly highlights the protective feature of hydrodynamic lubrication.

Again, for strips with pockets angle to the edge α = 10°, the same trend is observed but the effect of the pockets angle on the MPHDL onset discussed in the previous section is reinforced. Iftheincreaseofthedrawingvelocitytendstoincreasethe MPHDLphenomenon [5], it also tends to reduce the extent of the MPHSL [5]. The so-called *lubricant forward escape* [6] will be less far towards the contact exit (−x-direction) than when drawing at low velocity, and thus the ejected lubricant will remain close to its initial pocket and only lubricateitsleftedge. Analogouslytotheillustrationoffigure11b,theresultisadescendant slope for the profile of the peaks radius of curvature according the +x-position on the strips plateaus. Figure 12 shows this phenomenon through the multiscale decompositions related to testing conditions 10DTC2 and 10DTC4.

Figure 12: Multiscale decomposition of peaks and valleys curvature radii for conditions 10DTC2 (a) and 10DTC4 (b).

This is a pre-print of the paper published by Elsevier in Tribology International, Vol. 82 part B (2015) p. 375-386
kris@kubiak.co.uk
https://doi.org/10.1016/j.triboint.2014.04.035

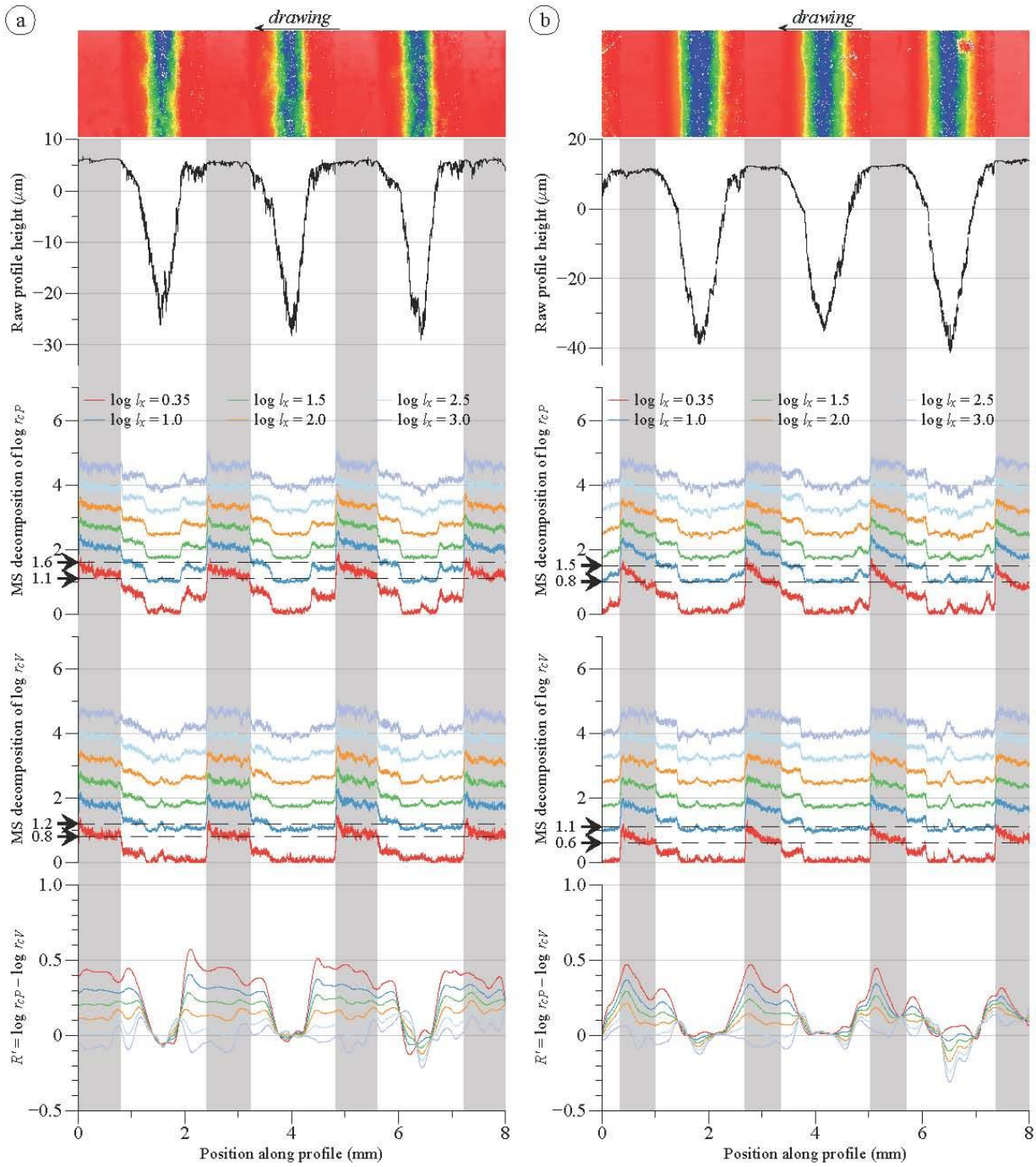

Figure 12: Multiscale decomposition of peaks and valleys curvature radii for conditions 10DTC2 (a) and 10DTC4 (b).

According to figure 12, it can be seen that the maximum value of log r_{cP} is slightly 19

This is a pre-print of the paper published by Elsevier in Tribology International, Vol. 82 part B (2015) p. 375-386
kris@kubiak.co.uk https://doi.org/10.1016/j.triboint.2014.04.035

decreased (from log $r_{cP} \approx 1.6$, $r_{cP} \approx 39.81\mu m$ at low velocity to log $r_{cP} \approx 1.5$, $r_{cP} \approx 31.62\mu m$), but the minimal value on the strips plateaus decreased with the increase of the velocity (from log $r_{cP} \approx 1.1$, $r_{cP} \approx 12.59\mu m$ at low velocity to log $r_{cP} \approx 0.8$). Along with the decreased values of log r_{cV} , the curvature radii measured for this testing condition are very close to the curvature radii of the initial profiles, especially in the right region of the strips plateaus. It shows that initial surfaces have not undergone severe contact conditions and thus contact pressure, contrarily to the opposite side of the plateaus.

4.3. Identification of lubrication regimes by means of the curvature radii

From a global point of view, the lubrication regimes involved in a strip drawing process can be estimated by means of process parameters and global measurements, such as the lubricant viscosity and the drawing forces, and their influence on the resulting friction coefficient. This influence has been described by Stribeck, and is commonly known as Stribeck's curve. In the case of this study, it is possible to plot such a curve, after friction coefficient calculation, and to estimate the global lubrication regime involved during the drawing operation of each specimen.

Two friction coefficients should ideally be identified, one for each tool surface. The testing device allows, however, only determination of one value based on measurements of the drawing force and inverse analysis using the slab method, implying that an average friction coefficient will be assumed.

Each testing configuration is plotted on the graph of figure 13. It must be noted that configuration 10DTC1 is not plotted since no stable regime (in terms of drawing force) has been reached during the tests, because of important sticking of aluminium strips to the glass die.

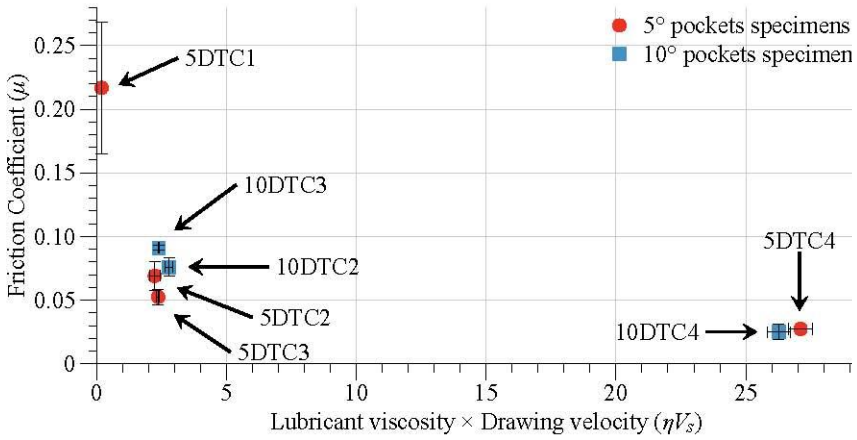

Figure 13: EvFigure 13: Evolution of the global friction coefficient according to the drawing velocitbricant viscosity, for eviscosity, for each test configuration.

Except for testing condition 5DTC1, it can be seen that the tests are quite repeatable. The major error source is from the drawing force sensor while the drawing velocity remain 20

stable for each test reproduction. Also, in terms of global values, the graph shows that the role played by the pockets angle is minimal: the global friction coefficient is slightly increased for low values of ηV_s and pockets angle $\alpha = 10^{\circ}$, which is, however, consistent with the analysis made in section 4.1.

From this graph and according to the shape of Stribeck's curve, the lubrication regime encountered for each testing condition can be estimated: mixed for testing conditions 5DTC2, 5DTC3, 10DTC2 and 5DTC3, mixed with a trend to boundary lubrication for testing condition 5DTC1 and a strong trend to hydrodynamic lubrication for conditions involving the high viscosity lubricant and the high drawing velocity, namely 5DTC4 and 10DTC4.

As explained in introduction of this paper and as shown by Bech et al. [5], local changes in lubrication regimes may occur because of MPHDL and MPHSL occurrence. Sections 4.1 and 4.2 highlighted these local changes in terms of peaks and valleys curvature radii, but these analyses are relative, based on comparisons of different testing conditions. They are important for the understanding of the contact lubrication and the effects of the drawing conditions on the lubrication, but the local lubrication regimes have not been estimated and this cannot be only based on the radius of curvature of peaks or valleys.
Still based on comparisons, another region of the specimens can be useful to make a step forward in the analyses: regions outside of the pockets row, as illustrated in figure 14.

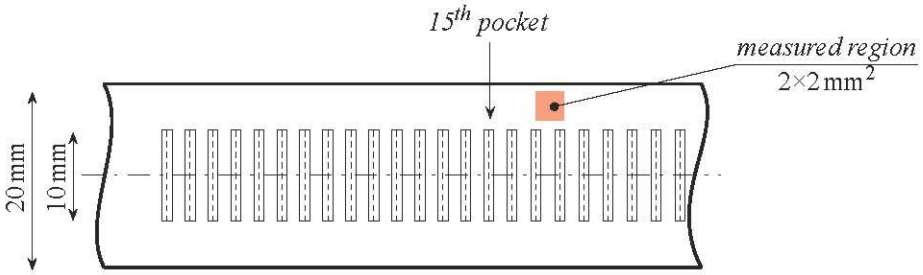

Figure 14: Location of measurements performed outside of the pockets row. row.

This measurement location is not affected by the pockets network and thus the measured surfaces have been deformed with constant lubrication regime. The measured surfaces are also longer than the plateaus, with the same width, that will allow to average the values of the peaks and valleys curvature radii. The averaged values of log r_{cP} and log r_{cV} and the value of the ratio of curvature radii $R^{\blacklozenge}$ are given in table 2, for all lubricant viscosities and drawing velocities combinations. Each combination is given a name similar to that used in table1, withouttheanglevaluesincethepocketsdonotplayanyroleinthesemeasurements.

A first look at the values of peaks curvature radius shows that they are consistent with the analyses of strips with pockets angle $\alpha = 5^{\circ}$ detailed in section 4.1. Concerning the curvature radius of valleys, they are slightly higher in regions out of the pockets row. This means that contact is more severe when no additional lubricant is provided in between the

This is a pre-print of the paper published by Elsevier in Tribology International, Vol. 82 part B (2015) p. 375-386
kris@kubiak.co.uk https://doi.org/10.1016/j.triboint.2014.04.035

Table 2: Averaged values of peaks and valleys curvature radii for all lubricant viscosities and drawing velocities combinations.

	TC1	TC2	TC3	TC4
log r_{cP}	1.51 ± 0.23	1.24 ± 0.22	1.26 ± 0.21	0.88 ± 0.17
log r_{cV}	1.28 ± 0.20	1.16 ± 0.17	1.08 ± 0.17	0.87 ± 0.14
$R^{\blacklozenge}$	0.234	0.122	0.177	0.005

contacting surfaces. On the contrary, in the case of strips with pockets angle α = 10°, the curvature radii measured on the plateaus are higher than outside of the pockets row, which is supposed to be due to the stiff pocket angle, that reduces the MPHDL effects as discussed in sections 4.1 and 4.2.

As introduced in section 3.2, the ratio of peaks and valleys curvature radii in logarithmic scale (equation (6)) is here of great interest: it gives an indication on the morphology of the surface peaks and valleys that can be linked to the contact severity and thus, an indication of the lubrication regime can be given.

As recalled in introduction, a mixed lubrication regime corresponds to few dry contacts between the tool/workpiece surfaces and a thin lubricant film in between these surfaces. Hydrodynamic lubrication is activated when there is almost no contact between the surfaces and, the opposite lubrication regime is the boundary regime, which takes place if the lubricant film is nearly broken. An illustration of these three main lubrication regimes is given in figure 15.

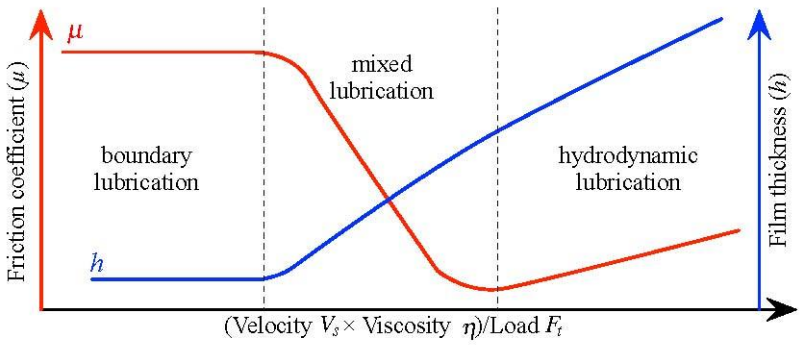

Figure 15: Illustration of the main three lubrication regimes.

The initial strips plateaus have homogeneous peaks and valleys curvature radii, thus $R^{\blacklozenge} \approx 0$ for log l_x=0.35. Based on the graph of figure 13, assuming that the expected mixed lubrication regime is reached outside of the pockets row for tests in condition TC1, leading to $R^{\blacklozenge}$=0.234 with increased values of log r_{cV}, and if the lubrication regime obtained with condition TC4 is assumed hydrodynamic, with $R^{\blacklozenge}$=0.005 and values of log r_{cV} close to the initial ones, thus the other values of $R^{\blacklozenge}$ obtained in the different testing conditions can be

This is a pre-print of the paper published by Elsevier in Tribology International, Vol. 82 part B (2015) p. 375-386
kris@kubiak.co.uk https://doi.org/10.1016/j.triboint.2014.04.035

classified and related, qualitatively, to a lubrication regime.

For testing condition 5DTC1, as illustrated in figure 9, R' ranges between 0.45 and 0.65, with lower log r_{cv} than for regions outside the pockets row. This means that the contact was less severe for this testing condition and confirms the protective effect of the lubricant reservoirs. This contact lubrication would range between mixed and hydrodynamic (undeformed valleys and eroded peaks). More generally, all tested configurations with $\alpha = 5^{\circ}$ give the same range for R': close to 0.5 for the low viscosity lubricant, smaller values for the high viscosity lubricant, around $R' = 0.35$ with values of log r_{cv} close to the initial ones.

It is more interesting to observe the strips plateaus for testing configurations with $\alpha = 10^{\circ}$, for which the profiles of curvature radii were not uniform. Taking the example of testing condition 10DTC2 (illustrated in figure 12a), on the strips plateaus R' varies in the range [0.32, 0.42], while for 10DTC4 (illustrated in figure 12b) R' varies in the range [0.25, 0.45] with smaller values of log r_{cv}. The postulated reason for this change in curvature radii was the effect of the stiff pockets angle limiting the hydrodynamic lubrication, leading to severe contact on the left side of the plateaus (high values of R' with high values of log r_{cv}), and soft, well lubricated contact on the right side of the plateaus (figure 11b, small values of R' with values of log r_{cv} close to the initial ones). In terms of ratio of curvature radii and for condition 10DTC4, the left regions of the plateaus have a ratio $R' \approx 0.45$ with high values of log r_{cv}, while the opposite side, where MPHSL has lubricated the contact, have a ratio $R' \approx 0.25$. Both regions of the plateaus can be assigned a mixed lubrication regime, but the combination of parameters R' and $\log_{r_{cV}}$ allows to highlight the local change in surface topography, and thus the contact conditions, due to the involved lubricant escape phenomenon, namely MPHSL and MPHDL.

5. Conclusion

In this paper, a fractal approach of the curvature radius has been applied, on the basis of experimental tests and measurements. The aim was to analyse the effects of aluminium strips drawing process conditions on the final surfaces state and local changes in lubrication regime. After multiscale decomposition of the profile peaks and valleys curvature radii, the results corresponding to each testing configuration are compared to quantify the effects of change of lubricant viscosity, drawing velocity and lubricant pockets angle on the curvature radii of both peaks and valleys. These two parameters, in addition to a third one which is the ratio between the first two parameters, are used as indicator of contact severity: the higher the radius of curvature, the higher the contact pressure was during plastic deformation. Then, by comparison with regions of the specimens that have been deformed without any effect of the lubricant pockets, the different lubrication regimes encountered in the tribological contact have been determined qualitatively.

The approach applied in this paper seems to be quite relevant and accurate to distinguish the regions where different contact conditions occurred. Nevertheless, the authors will delve into each initial configuration, their profiles, roughness and curvature radii to eventually be more accurate in the identification of contact properties and lubrication regimes. It is also

necessary to perform more basic experiments to establish more solid grounds for further investigations.

6. Acknowledgements

Authors would like to thank Professor Niels Bay from Technical University of Denmark for providing experimental support for tribological drawing tests and stimulating scientific discussions.
ThepresentresearchworkhasbeensupportedbytheInternationalCampusonSafetyand Intermodality in Transportation, the Nord-Pas-de-Calais Region, the European Community, the Regional Delegation for Research and Technology, the Ministry of Higher Education and Research, and the National Centre for Scientific Research. The authors gratefully acknowledge the support of these institutions.

7. References

[1] S. M. Bloor, D. Dowson, B. Parsons, An elasto-plasto-hydrodynamic lubrication analysis of the plane strain drawing process, Journal of Mechanical Engineering Science 12 (3) (1970) 178 – 190.
[2] H.Kudo,M.Tsubouchi,H.Takada,K.Okamura,Aninvestigationintoplasto-hydrodynamiclubrication with a cold sheet drawing test, CIRP Annals -Manufacturing Technology 31 (1) (1982) 175 – 180.
[3] T. Mizuno, M. Okamoto, Effects of lubricant viscosity at pressure and sliding velocity on lubricating conditions in the compression-friction test on sheet metals, Journal of Lubrication Technology 104 (1) (1982) 53–59.
[4] A. Azushima, H. Kudo, Direct observation of contact behaviour to interpret the pressure dependence of the coefficient of friction in sheet metal forming, CIRP Annals -Manufacturing Technology 44 (1) (1995) 209 – 212.
[5] J. Bech, N. Bay, M. Eriksen, Entrapment and escape of liquid lubricant in metal forming, Wear 232 (2) (1999) 134–139.
[6] L. Dubar, C. Hubert, P. Christiansen, N. Bay, A. Dubois, Analysis of fluid lubrication mechanisms in metal forming at mesoscopic scale, CIRP Annals -Manufacturing Technology.
[7] B. Lee, Y. Keum, R. Wagoner, Modeling of the friction caused by lubrication and surface roughness in sheet metal forming, Journal of Materials Processing Technology 130–131 (0) (2002) 60 – 63.
[8] H. Gong, Z. Lou, Z. Zhang, Studies on the friction and lubrication characteristics in the sheet steel drawing process, Journal of Materials Processing Technology 151 (1–3) (2004) 328 – 333.
[9] H. Christensen, Stochastic models for hydrodynamic lubrication of rough surfaces, Proceedings of the Institution of Mechanical Engineers 184 (1) (1969) 1013–1026.
[10] H. Le, M. Sutcliffe, Measurements of friction in strip drawing under thin film lubrication, Tribology International 35 (2) (2002) 123 – 128.
[11] H. Costa, I. Hutchings, Effects of die surface patterning on lubrication in strip drawing, Journal of Materials Processing Technology 209 (3) (2009) 1175 – 1180.
[12] M. Bigerelle, J. Nianga, D. Najjar, A. Iost, C. Hubert, K. Kubiak, Roughness signature of tribological contact calculated by a new method of peaks curvature radius estimation on fractal surfaces, Tribology International (65) (2013) 235–247.
[13] B. B. Mandelbrot, J. R. Wallis, Computer experiments with fractional gaussian noises. part 1, sample graphs, averages and variances, Water Resources Research 10 (1969) 228–241.
[14] K. Kubiak, M. Bigerelle, T. Mathia, A. Dubois, L. Dubar, Dynamic evolution of interface roughness during friction and wear processes, Scanning (in press). doi:10.1002/sca.21082.

[15] C. Hubert,P. C.N.Bay,R.Deltombe,L.Dubar,M.Dubar,A.Dubois,Numericalsimulationoflubrication mechanisms at mesoscopic scale, in: Proceeding of the 14th International ESAFORM Conference, AIP Conference Procedings, 2011, pp. 1729–1734.
[16] Zygo NewView 7300 web page [link].
[17] B. Nowicki, Multiparameter representation of surface roughness, Wear 102 (3) (1985) 161 – 176.
[18] C. Sørensen, J. Bech, J. Andreasen, N. Bay, U. Engel, T. Neudecker, A basic study of the influence of surface topographyon mechanismsofliquid lubricationinmetal forming, CIRPAnnals -Manufacturing Technology 48 (1) (1999) 203 – 208.

.....

.....û..... .....

.....

蠱椀最甄嫲攀.....